

Mechanism of Traditional Chinese Medicine in the Treatment of Ischemic Stroke by Intervening Ferroptosis Pathway Based on Molecular Target Prediction and Bioinformatics

Wang Chang Zhong¹, Sun Zijin² and Zhou Wei^{3*}

¹Department of Medicine, Graduate School of Tianjin University of Traditional Chinese Medicine, Tianjin, China

²Department of Materia Medica, School of Chinese Materia Medica, Beijing University of Chinese Medicine, Beijing, China

³Department Chinese Medicine, The Second Affiliated Hospital of Tianjin University of Traditional Chinese Medicine, Tianjin, China

Abstract

Objective: The study employed bioinformatics, molecular docking, and molecular dynamics techniques to identify genes and targets involved in ischemic stroke through the ferroptosis pathway.

Methods: Gene data from the Gene Expression Omnibus (GEO) and FerrDb platform were integrated and analyzed, resulting in 410 related genes. After differential analysis and RF algorithm sorting, nine key genes were identified, showing significant correlation with immune cells and inflammatory factors.

Results: Traditional Chinese medicine (TCM) components corresponding to these genes were screened using Symptom Mapping, yielding 445 TCMs and 1799 small molecule ligands. Molecular docking validated 10,850 active ingredient-target combinations, with ECH1-118705169 and ECH1-Kaempferol-3,7-O-bis-alpha-L-rhamnoside exhibiting stable binding in molecular dynamics simulations.

Conclusion: The study concluded a substantial correlation between ferroptosis and ischemic stroke, highlighting TCMs' role in regulating liver, lung, stomach, and spleen functions to interfere with ferroptosis. Notably, bitter and cold medicines, followed by sweet and warm products, play significant roles in heat clearing, detoxification, and inhibiting lipid peroxidation or inflammation. The stable binding of specific TCM components suggests further exploration of their molecular mechanisms. Overall, these findings serve as a valuable reference for developing curative strategies and advancing traditional Chinese medicine research.

Keywords: Ischemic stroke; Ferroptosis; Bioinformatics; Molecular docking; Molecular dynamics; Traditional Chinese medicine

Introduction

Ferroptosis is a novel cell death mode with abnormal iron metabolism proposed by Brent Stockwell in 2012 [1]. The primary ferroptosis mechanism is the reaction of intracellular free-divalent Fe^{2+} with hydrogen peroxide to generate Fe^{3+} [2], causing lipid peroxidation of unsaturated fatty acids [3,4], ultimately promoting oxidative stress-mediated cell death. There are no morphological characteristics for apoptosis or exhibit the phenomena that occur in traditional apoptosis in ferroptosis, like cell shrinkage, chromatic agglutination, generation of apoptotic bodies, or the disintegrated cytoskeleton. However, by electron microscopy, it can be showed that mitochondria shrink significantly with increased membrane density [5], whose characteristic is a large accumulation of oxygen species and intracellular iron, as well as iron-dependent consumption and excessive neutralization of glutathione peroxidase 4, resulting in an abundance of free radicals and damage to cell membrane lipids due to oxidation. Evidence shows that ferroptosis can be induced by inhibiting cystine glutamate transporter, promoting p53 gene expression, directly inhibiting GPX4, and interfering with VDACs (Voltage Dependant Anion Channels) [6].

Ischemic Stroke (IS) refers to the thrombosis of the inner wall of the blood supply vessels to the brain, which blocks the arteries after falling off, resulting in insufficient blood supply and necrosis of the brain, accounting for about 80% of all stroke patients [7]. Numerous research investigations have established a strong connection between ferroptosis and its pivotal involvement in ischemic stroke.

Limited research has been conducted on the intervention of components from traditional Chinese medicine in the context of

ferroptosis. However, some small molecular components derived from natural drugs have been proven to scavenge free radicals and block lipid peroxidation as free radical scavengers, thereby blocking ferroptosis. For example, after quercetin treatment, the expression of ferroptosis induced by erastin can be diminished by bone marrow mesenchymal stromal cells [8]. Puerarin can effectively inhibit iron overload and lipid peroxidation, suppress ferroptosis, and alleviate heart damage in rat cardiomyocytes and rat arterial ligation models [9]. Moreover, Gastrodin can diminish oxidative stress and peroxide levels in HT-22 cells. This is achieved by up-regulating Nuclear Factor Erythroid 2-Related Factor 2 (Nrf2), enhancing Heme Oxygenase 1 (HO-1), and promoting Glutathione Peroxidase 4 (GPX4). Consequently, this helps in preserving against glutamate-induced ferroptosis [10]. However, there are few studies on the treatment of IS by traditional Chinese medicine drugs through the intervention of ferroptosis. This study hopes to clarify the gene target of IS from ferroptosis through bioinformatics and screen traditional Chinese medicine drugs that may

***Corresponding author:** Dr. Zhou Wei, Department Chinese Medicine, The Second Affiliated Hospital of Tianjin University of Traditional Chinese Medicine, Tianjin, China, E-mail: 1020263993@qq.com

Received: 28-Mar-2024, Manuscript No. DPO-24-130902; **Editor assigned:** 01-Apr-2024, PreQC No. DPO-24-130902(PQ); **Reviewed:** 15-Apr-2024, QC No. DPO-24-130902; **Revised:** 22-Apr-2024, Manuscript No. DPO-24-130902(R); **Published:** 29-Apr-2024, DOI: 10.4172/2476-2024.1000229

Citation: Zhong WC, Zijin S, Zhou W (2024) Mechanism of Traditional Chinese Medicine in the Treatment of Ischemic Stroke by Intervening Ferroptosis Pathway Based on Molecular Target Prediction and Bioinformatics. *Diagn Pathol Open* 9:203

Copyright: © 2024 Zhong WC, et al. This is an open-access article distributed under the terms of the Creative Commons Attribution License, which permits unrestricted use, distribution, and reproduction in any medium, provided the original author and source are credited.

have intervention effects to provide ideas for clinical treatment.

Materials and Methods

Collection and pretreatment of IS gene data sets

The dataset GSE16561 and dataset GSE58294 are obtained from the GEO (<https://www.ncbi.nlm.nih.gov/gds/>). The Limma package of R language (version 4.2.3) was used to internally standardize each dataset to reduce the batch effect of sequencing depth and gene attributes, and log₂ transformation of gene expression. The SVA package was used to de-batch the genes that co-exist between the two data sets, and the Principal Component Analysis (PCA) diagram was used to show the difference before and after.

Ferroptosis-related gene collection and single sample Gene Set Enrichment Analysis (ssGSEA)

The FerrDb platform is a database that collects ferroptosis regulatory factors, marked factors, and ferroptosis-related diseases. Genes associated with ferroptosis were collected through the FerrDb platform (<http://www.zhounan.org/ferrdb/>). The ssGSEA method in the GSVA (Gene Set Variation Analysis) was used to score the expression of these genes in each sample, and the differences between the standard group and the IS group were analyzed to observe whether ferroptosis had a difference in gene expression between the two groups.

Differential analysis of ferroptosis gene dataset and acquisition of key genes

The Limma package was used to analyze the differential genes in the ferroptosis gene dataset, and $P(\text{adj}) < 0.05$ was set as the screening standard for differential genes. The algorithm utilized for ranking the importance of the obtained differential genes included the Support Vector Machine (SVM) and Random Forest (RF). The above algorithm was used to obtain the top 15 in the rank, and the intersection was taken to obtain the key genes. The key genes and the genetic correlation in IS samples were analyzed.

Immune infiltration analysis

The relative content of each immune cell and inflammatory factor in each sample was calculated by the CIBERSORT package as the result of immune infiltration. The outcomes were employed to derive variations in the relative content of immune cells and inflammatory factors among distinct groups, and the correlation between key genes and relative content was further obtained to find out the key genes related to immune regulation in this process.

Cluster analysis and cluster subgroup information comparison

The Consensus Cluster Plus package got the consensus scoring on key genes. Cluster analysis was based on these results, and clinical-related information was compared among different cluster subgroups to observe the clinical phenotypes of different groups. Genes with $P(\text{adj}) < 0.05$ and $|\log FC| \geq 0.5$ in different subgroups were selected and transformed into protein names, and protein functional clustering was performed using the proteomaps database.

Screening and analysis of traditional Chinese medicine corresponding to core targets

The core genes were input into the symmap database to find the corresponding small molecule active ingredients and traditional Chinese medicines. According to 'Chinese Pharmacopoeia', 'Chinese

Materia Medica', and 'The Dictionary of Chinese Herbal Medicine', the properties, flavors, meridian tropism and drug classification of traditional Chinese medicine were statistically analyzed. Cytoscape V 3.9.1 was used to construct the 'target-traditional Chinese medicine' network and obtain the core traditional Chinese medicine through topological analysis.

Molecular docking

Molecular docking was performed using MGLTools 1.5.7 and AutoDock 4.2.62 tools. The docking process was as follows: First, the three-dimensional structure of the protein was retrieved from the Protein Data Bank database (PDB, <http://www.rcsb.org/pdb>) and converted into a PDBQT protein receptor file. Then the small molecule ligand file was downloaded from the PubChem database (<http://pubchem.ncbi.nlm.nih.gov/>), modified, and saved as a PDFBQT ligand file. After setting the parameters such as pairing pocket and docking times, the active ingredient (ligand) was docked with the target (receptor). Finally, Discovery Studio (DS, V2019) was used for visualization.

Molecular dynamics simulation and evaluation

For the stability of the obtained ligand-acceptor combination, GROMACS software was used to perform 50 ns molecular dynamics simulations on the ligand-acceptor conformations with the top 5 molecular docking binding energies. First, the PDB file of the target protein (receptor) was processed to generate the relevant topology. SwissParam then treated the small molecules (ligands). The information on small molecular substances was added to the protein topology file to form a compound information file. The charmm 36 force field and TIP3P water model were used to calculate, and the cube with a size of 1.2 was set as the limiting box.

Then the solvent (SPC216 water) was added to it. Na⁺/Cl⁻ ion pairs were introduced into the system to equilibrate the charge. Because the collision between proteins and small molecules, the steepest descent method was used to optimize the system to achieve the optimal potential energy. The regular system was balanced at 300 K, and the isothermal, isobaric system was balanced under Parrinello-Rahman pressure coupling and 1 bar (1000 ps, the kinetic step was 2 fs). The system's coordinates and energy were stored at intervals of every 10 ps. Finally, after 50 ns simulation of each system, the molecular trajectory of the system was corrected to evaluate and calculate it.

Calculation of Molecular Mechanics Poisson-Boltzmann Surface Area (MMPBSA) binding free energy

By the binding free energy calculation method, the results obtained by the molecular dynamics trajectory were improved, and the affinity between the protein and the small molecule ligand was quantified numerically. The MMPBSA approach is extensively employed for computing the binding free energy, forecasting the resilience of the ligand-receptor post molecular dynamics simulation. A 50 ns molecular dynamics trajectory is employed in the computation, with the specific formula outlined as follows:

$$\Delta G_{\text{bind}} = \Delta G_{\text{complex}} - (\Delta G_{\text{receptor}} + \Delta G_{\text{ligand}}) = \Delta H - T\Delta S$$

$$\Delta H = \Delta E_{\text{MM}} + \Delta G_{\text{sol}}$$

$$\Delta E_{\text{MM}} = \Delta E_{\text{ele}} + \Delta E_{\text{vdW}} + \Delta E_{\text{int}}$$

Finally, the transformation formula is merged to obtain:

$$\Delta G_{\text{bind}} = \Delta E_{\text{int}} + \Delta E_{\text{vdW}} + \Delta E_{\text{ele}} + \Delta G_{\text{PB}} + \Delta G_{\text{SA}}$$

ΔG_{bind} represents the free energy of binding, $\Delta G_{\text{Gcomplex}}$ denotes the free energy of binding for the complex, $\Delta G_{\text{Greceptor}}$ signifies the free energy of binding for the receptor, $\Delta G_{\text{Gligand}}$ expresses the free energy of binding for the ligand, T Δ S stands for the entropy change value of the system, ΔH refers to the enthalpy variable, ΔE_{EMM} represents the gas phase energy, ΔG_{sol} signifies the energy associated with solvation, ΔG_{GPB} indicates the energy contribution from polar solvation, and ΔG_{GSA} stands for the energy associated with non-polar solvation. The internal energy of ΔE_{int} comprises bond energy, bond angle energy, and torsion energy. In this investigation, the conformational arrangement of proteins and small molecule ligands is acquired through a lone molecular dynamics trajectory, focusing solely on the trajectory of the complex. This treats the structure of the protein-small molecule ligand as a fixed entity. Consequently, the ΔE_{int} between the complex and the individual components (i.e., the protein and the small molecule ligand) can offset each other due to the calculation of the energy term in the same molecular dynamics simulation trajectory. As a result, this study exclusively delved into specific research on ΔE_{Ele} and ΔE_{vdW}

Results

The collection and pretreatment results of IS gene data sets

In our downloaded dataset GSE16561 and dataset GSE58294, the former had 24 IS samples and 39 standard samples, while the latter had 31 IS samples and 23 standard samples. After the standardization within the data set and the batch removal between the data sets, it can be seen from the Figure 1 that the two data sets have removed the batch effect and can be analyzed in the next step.

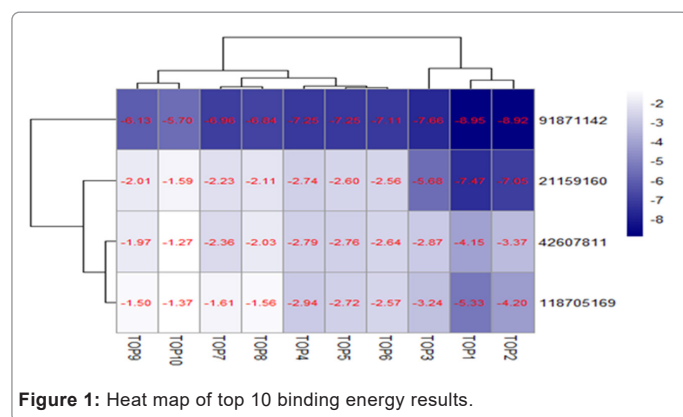


Figure 1: Heat map of top 10 binding energy results.

The ferroptosis-related gene collection and ssGSEA results

Through the Ferrdb platform, we obtained 565 genes, of which 410 genes have relevant information in the integrated data set. We used the ssGSEA method in the GSVA package to perform Wilcoxon analysis on the standard group and the IS group. It was found that the ferroptosis-related genes were highly expressed in the IS group.

Statistical differences

The differential analysis results of ferroptosis gene dataset and acquisition of key genes: Following the analysis of variations, a sum of 182 differential genes was acquired, comprising 121 genes exhibiting an increase in expression and 70 genes displaying a decrease in expression. The top 15 key genes obtained by the SVM algorithm were Lysosomal Associated Membrane Protein 2 (*LAMP2*), Solute Carrier Family 2 Member 3 (*SLC2A3*), Bromodomain Containing 2 (*BRD2*), Phosphatase And Tensin Homolog (*PTEN*), Zinc Finger Protein (*ZNF419*), Mitogen-Activated Protein Kinase 14 (*MAPK14*), Arachidonate 5-Lipoxygenase

(*ALOX5*), *PHF21 A*, Ribosomal Protein L8 (*RPL8*), Dual Specificity Phosphatase 1 (*DUSP1*), Thioredoxin (*TXN*), Serine/Threonine Kinase (*ATM*), ATP Binding Cassette Subfamily C Member 1, (*ABCC1*), Acyl-CoA Synthetase Long Chain Family Member 1 (*ASCL1*), Enoyl-CoA Hydratase 1 (*ECH1*); the RF algorithm is used to rank the importance of genes by using Mean Decrease Gini, and the results are shown in the Figure 2. It can be seen from the box plot that the expression of these genes in the two groups of samples was statistically different. According to the heat map of gene correlation, among the nine key genes in IS samples, *ALOX5* had the strongest positive correlation with *SLC2A3*, while *BRD2* and *TXN* genes had the strongest negative correlation.

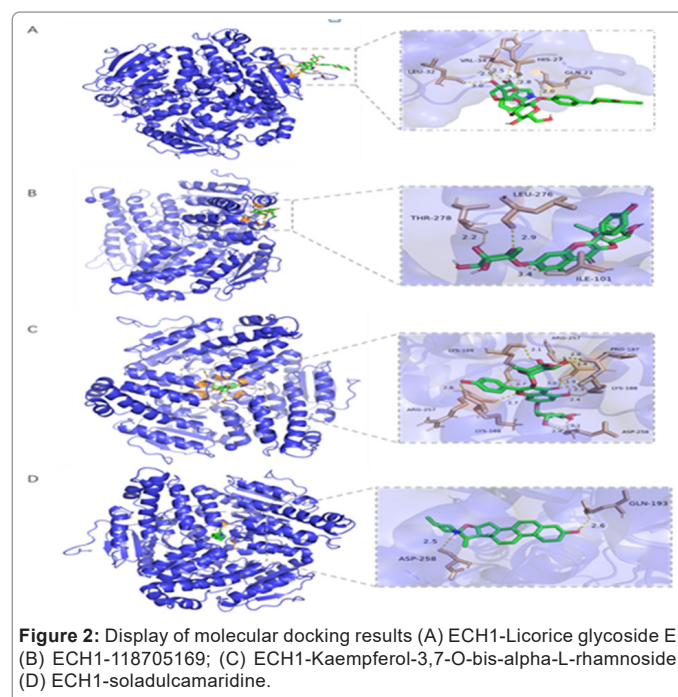


Figure 2: Display of molecular docking results (A) ECH1-Licorice glycoside E; (B) ECH1-118705169; (C) ECH1-Kaempferol-3,7-O-bis-alpha-L-rhamnoside; (D) ECH1-soladulcamaridine.

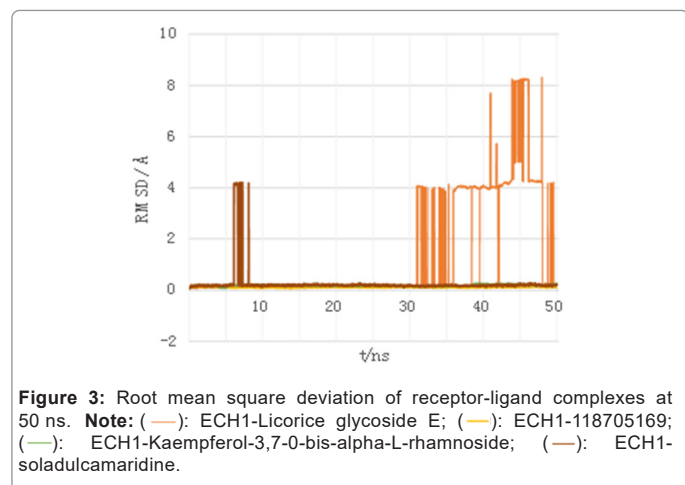
The immune infiltration analysis results

Through analysis of immune infiltration, it was observed that in the IS group, there was a relatively low presence of naive B cells, memory B cells, CD8(+) T cells, naive CD4(+) T cells, resting CD4(+) memory T cells, and active natural killer cells. In contrast, the IS group exhibited a relatively high abundance of active CD4(+) memory T cells, inactive natural killer cells, monocytes, M0 macrophages, and neutrophils. The relative contents of CD4(+), *HLA-DRA*, *TGFB3*, and *TNF* in the IS group were low, and the relative contents of *IFNA1*, *IL10*, *IL15*, and *IL1 A* in the IS group were high. The nine key genes are significantly correlated with a variety of immune cells and inflammatory factors, which proves that these key genes may regulate the immune-related phenotype of the disease.

The results of cluster analysis and cluster subgroup information comparison

According to the expression of 9 key genes, the IS samples were divided into subgroup 1 and subgroup 2 by cluster analysis. It can be seen from the Figure 3 that the IS samples are mostly male in subgroup 1, and the onset time is primarily short, concentrated in the 3-hour interval; subgroup 2 was predominantly female, and the onset time was relatively long, concentrated in the 5-hour interval. The relative expression of *TXN*, *LAMP2*, *MAPK14*, *ALOX5*, and *SLC2A3* genes were lower in subgroup 1, while *ABCC1* and *ZNF419* were higher in

subgroup 1. The expression differences of these genes may be related to the clinical phenotype of the subgroup. In addition, the comparative content of naive B cells, memory B cells, CD8(+) T cells, active NK cells, resting mast cells, and active dendritic cells were higher in subgroup 1. In contrast, one of M0 macrophages, active mast cells, and neutrophils were higher in subgroup 2. From the perspective of inflammatory factors, the comparative contents of *HLA-DRA*, *IL10*, *IL15*, and *TGFB3* were higher in subgroup 1, while the comparative contents of *CSF3*, *TGFB1*, and *TGFB2* were higher in subgroup 2.



The screening and analysis results of traditional Chinese medicine corresponding to core targets

After using symmap to analyze the key genes, 445 corresponding traditional Chinese medicines were obtained, and the Four Qi, Five Flavors, and Meridian tropism were analyzed. The corresponding frequency of the Four Qi was: Cold (163)>warm (129)>flat (99)>cool (44)>hot(10). The corresponding frequency of the five flavors was: Bitter (249)>sweet (179)>pungent (169)>astringent (37)>acid (34)>salty (22)>weak (13). The corresponding frequency of meridian tropism was: Liver (232)>lung (179)>stomach (141)>spleen (129)>kidney (108)>heart (91)>large intestine (73)>bladder (38)>gallbladder (23)>small intestine (17)>pericardium (5)>triple energizer(3). Core Chinese medicine (degree value >2 times the median) mainly includes: Haijinsha, Fengfang, Baiguo, Gancao, Gouguyue, Huzhang, Laoguancao, Zaojiaoci, Huajiao, Maoyancao, Yujin, Kuxingren, Mohanlian 13 herbs.

Molecular docking results

After the small molecule ligands and protein receptors were downloaded and modified to pdbqt, 1799 (1206 were successfully downloaded) small molecule ligands (core Chinese medicine active ingredients) and 9 protein receptors were obtained. They were LAMP2 (PDB ID: 2MOF), SLC2A3 (PDB ID: 7SPT), BRD2 (PDB ID: 5IG6), ZNF419 (Entrez Gene ID: 79744), MAPK14 (PDB ID: 2FST), ALOX5 (PDB ID: 3O8Y), TXN (PDB ID: 1AIU), ABCC1 (PDB ID: 2CBZ), ECH1 (PDB ID: 2VRE). Finally, 10850 protein receptor-small molecule ligand combinations were successfully docked.

In practice, binding energy is often used to evaluate the affinity of the receptor and the ligand. It is generally believed that the binding energy less than -4.25 , -5.0 , or -7.0 kcal/mol ($1 \text{ kcal}=4.2 \text{ kJ}$) indicates a certain, good, or strong binding activity between the receptor and the ligand, respectively. Binding energy reflects the possibility of receptor binding to a ligand. The lower the binding energy, the higher the affinity

of the receptor and the ligand, and the more stable the conformation. The results of this study show that there are 11813 acceptor-ligand combinations with binding energy ≤ -4.25 kcal/mol, 10694 acceptor-ligand combinations with binding energy ≤ -5.0 kcal/mol, and 5481 acceptor-ligand combinations with binding energy ≤ -7.0 kcal/mol, indicating that most acceptor-ligand combinations can work well. The top 10 receptor-ligand combinations were ECH1-Licorice glycoside E (CID: 42607811), ECH1-Kaempferitrin (CID: 44258935), ECH1-5-hydroxy-2-(4-hydroxyphenyl)-7-[(2S, 3R, 4R, 5R, 6S)-3,4,5-trihydroxy-6-methyloxan-2-yl] oxy-3-[(2R, 3R, 4R, 5R, 6S)-3,4,5-trihydroxy-6-methyloxan-2-yl] oxychromen-4-one (CID:118705169), ECH1-Kaempol-3,7-O-bis-alpha-L-rhamnoCHside (CID:21159160), ECH1-Soladulcamaridine (CID:91871142), ECH1-Furosin, ECH1-Lespenefril, ECH1-Quercetin 3-O-rhamnoside 7-O-glucoside, ECH1-Liquiritin apioside, ALOX5-Licorice glycoside E. The complex binding can be seen in Table 1. The receptor-ligand combination with the top 5 binding energy was selected for molecular docking simulation. Among them, the ECH1-Kaempferitrin receptor-ligand combination could not be docked due to the small molecular structure of Kaempferitrin. The docking results of the other four groups of complexes with the top 10 binding energy were shown in Figure 4. In these four receptor-ligand combinations, all the receptor was ECH1, indicating that ECH1 can form a more stable conformation with small molecule ligands (Figure 5), thus playing a role.

Receptor-ligand combinations	molecular docking binding energies
ECH1- Licorice glycoside E	-12.5
ECH1- Kaempferitrin	-11.9
ECH1 118705169	-11.6
ECH1-Kaempferol-3,7-O-bis-alpha-L rhamnoside	-11.6
ECH1 Soladulcamaridine	-11.6
ECH1 Furosin	-11.5
ECH1 Lespenefril	-11.5
ECH1 -Quercetin 3-O-rhamnoside 7-O-glucoside	-11.5
ECH1 Liquiritin apioside	-11.4
ALOX5-Licorice glycoside E	-11.4

Table 1: Top 10 receptor-ligand combinations of molecular docking binding energies.

Molecular dynamics results

Root Mean Square Deviation (RMSD): The RMSD in molecular dynamics simulations mirrors the motion dynamics of the protein-small molecule ligand complex. The greater the RMSD of the complex, the more pronounced the fluctuations, indicating increased instability. Conversely, a lower RMSD suggests a more stable complex system. Among them, the RMSD of ECH1-118705169 and ECH1-Kaempferol-3,7-O-bis-alpha-L-rhamnoside complexes steadily came together

during the initial 5 ns of the simulation and sustained a comparatively consistent variability in the subsequent simulation. The RMSD of ECH1-Soladulcamaridine also sustained a comparably steady variation after the 6-8 ns fluctuation period, indicating that the movement of the three complex systems was stable after binding. In contrast, the RMSD of ECH1-Licorice glycoside E increased to a high level after binding for 30 ns, indicating that the complex system remained in a relatively unstable state. The stability of the above four complex systems from high to low is ECH1-Kaempferol-3,7-O-bis-alpha-L-rhamnoside>ECH1-118705169>ECH1-Soladulcamaridine>ECH1-Licorice glycoside E. The calculation results are shown in Figure 5.

Binding free energy: Utilizing the molecular dynamics simulation trajectory, the MMPBSA approach was employed to compute the binding free energy, providing a more precise depiction of the binding mode between the target protein and the small molecule (receptor-ligand). The adverse value signified the affinity of the small molecule to the target protein, and the diminished the value, the more robust the binding force. The calculation results showed that these small molecules had a particular binding affinity with the corresponding proteins and were very strong. The binding affinity of ECH1-Kaempferol-3,7-O-bis-alpha-L-rhamnoside was the highest, which was (-97.048 ± 1.876) kJ/mol (Table 2).

Hydrogen bond analysis: Hydrogen bonding stands as among the most potent non-covalent binding associations. An increased count of hydrogen bonds contributes to an enhanced binding effect. Figure 5 illustrates that the count of hydrogen bonds in the receptor-ligand complex was ECH1-Soladulcamaridine > ECH1-Licorice glycoside E>ECH1-Kaempferol-3,7-O-bis-alpha-L-rhamnoside>ECH1-118705169. From the number of hydrogen bonds presented in Figure 4, it could be inferred that hydrogen bonds may dominate the interaction of ECH1-Soladulcamaridine, ECH1-Licorice glycoside E, ECH1-Kaempferol-3,7-O-bis-alpha-L-rhamnoside. The interaction of ECH1-118705169 may not be through hydrogen bonds, but hydrophobic interactions.

Resilience of the target protein at the residue level: For the regional variations in macromolecular proteins at the residue level,

RMSF is introduced to depict the adaptability of proteins in molecular dynamics simulation. Typically, following the interaction of the drug with the protein, the adaptability of the protein decreases, leading to the stabilization of the protein and the manifestation of its enzymatic effect. The outcomes indicated a notably elevated RMSF in the ECH1-Licorice glycoside E complex compared to the other three groups, implying that the complex persisted in a comparatively precarious state. The peak and valley time of RMSF of the other three groups were similar. The fluctuation of RMSF of ECH1-Soladulcamaridine was higher than that of relatively stable ECH1-Kaempferol-3,7-O-bis-alpha-L-rhamnoside and ECH1-118705169, indicating that the three drugs had similar onset sites and may work through similar mechanisms. The calculation results of RMSF are shown in Figure 4.

Radius Of Gyration (ROG): Analysis of ROG reflects the tightness of receptor-ligand binding and can indicate the extent of constraints within the binding system. The ROG results of ECH1-Licorice glycoside E and ECH1-Soladulcamaridine complexes were consistent with the RMSD results, which were at a high level after 30 ns and 6-8 ns, respectively, indicating that the two complex systems were in a relatively unstable state during this period. The average ROG of ECH1-Soladulcamaridine, ECH1-118705169, and ECH1-Kaempferol-3,7-O-bis-alpha-L-rhamnoside receptor-ligand complexes was 2.7, indicating that the density of the system was high and the binding was tight. The calculation results are shown in Figure 6.

Solvent Accessible Surface Area (SASA) analysis: The solvent accessible surface area is computed based on the interface enclosed by the solvent. Solvents manifest diverse behaviors in various situations, making the solvent accessible surface area a valuable parameter for investigating the dynamics of protein conformation in the solvent milieu. The disparity in the solvent area of interaction within the four complexes steadily expanded post 10 ns. At 50 ns, the SASA from high to low was ECH1-Licorice glycoside E>ECH1-118705169>ECH1-Soladulcamaridine>ECH1-Kaempferol-3,7-O-bis-alpha-L-rhamnoside. However, the difference in this interval was relatively small, indicating that the effect of small molecules on protein targets was less affected by solvents. The results are shown in Figure 6.

Receptor-ligand combinations	van der Waals force / (kJ·mol ⁻¹)	Electrostatic potential / (kJ·mol ⁻¹)	Polar solvation energy/ (kJ·mol ⁻¹)	Solvent accessible surface area energy/ (kJ·mol ⁻¹)	Binding free energy/ (kJ·mol ⁻¹)
ECH1-Licorice glycoside E	182.234 ± 5.672	-96.019 ± 1.380	347.428 ± 1.4582	-26.782 ± 0.383	-4.297 ± 18.691
ECH1-118705169	-261.497 ± 1.492	-80.194 ± 1.226	344.457 ± 2.256	-26.043 ± 0.087	-23.286 ± 2.221
ECH1- Kaempferol-3,7-O-bis-alpha-L-rhamnoside	-241.478 ± 1.086	-24.751 ± 0.569	190.579 ± 1.795	-21.331 ± 0.075	-97.048 ± 1.876
ECH1- Soladulcamaridine	-255.885 ± 1.163	-97.018 ± 1.781	386.026 ± 1.973	-27.113 ± 0.093	-5.924 ± 2.364

Table 2: Binding free energy and energy value of each receptor-ligand complexes.

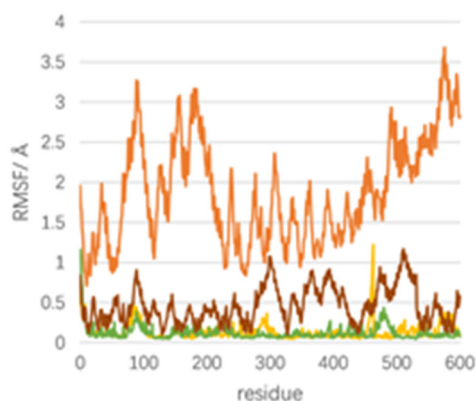


Figure 4: Root mean square fluctuation of receptor-ligand complexes at 50 ns. **Note:** (—): ECH1-Licorice glycoside E; (—): ECH1-118705169; (—): ECH1-Kaempferol-3,7-0-bis-alpha-L-rhamnoside; (—): ECH1-soladulcamaridine.

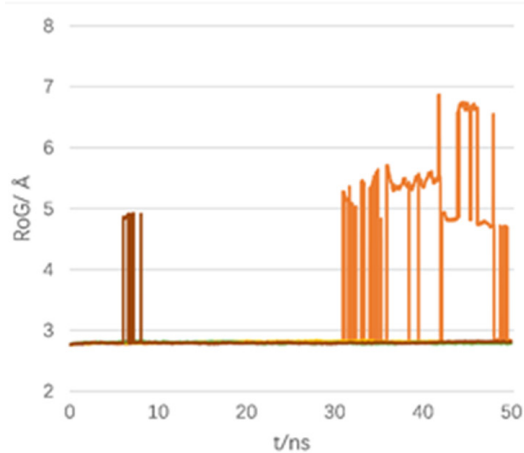


Figure 5: Calculation of 50 ns radius of gyration of receptor-ligand complexes. **Note:** (—): ECH1-Licorice glycoside E; (—): ECH1-118705169; (—): ECH1-Kaempferol-3,7-0-bis-alpha-L-rhamnoside; (—): ECH1-soladulcamaridine.

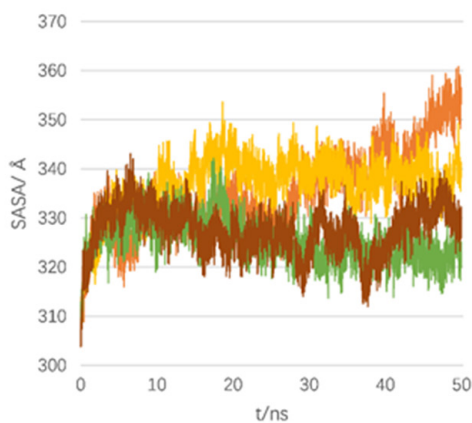


Figure 6: Solvent accessible surface area of receptor-ligand complexes at 50 ns. **Note:** (—): ECH1-Licorice glycoside E; (—): ECH1-118705169; (—): ECH1-Kaempferol-3,7-0-bis-alpha-L-rhamnoside; (—): ECH1-soladulcamaridine.

Discussion

As a refractory disease, IS is marked by a high frequency, elevated disability rate, increased mortality rate, and heightened recurrence rate [11,12]. The intricate pathological course and associated mechanisms have perpetually captured attention and research interest. Since ferroptosis was first proposed in 2012, related research has increased rapidly in the past decade. As of December 31, 2021, nearly 4000 papers in this field have been published, with an average citation frequency of 24.29 times. Although its physiological significance is still controversial, its role in a variety of major human diseases has received more and more attention. Current studies have found that the disorder of brain iron homeostasis is related to the acute neuronal injury of IS, which may be the primary mechanism of ferroptosis [13]. The acidic condition within brain tissue induced by cerebral ischemia can impede the attachment of iron ions to transferrin, leading to the liberation of iron ions from transferrin [14]. In addition, the decrease of iron ion efflux after IS may also be a significant cause of iron deposition [15-22]. Clinical studies have shown that after the occurrence of IS, the iron content in the ischemic area is significantly increased [19], and serum iron is also significantly increased [23].

Studies have found that Chinese herbal medicines contain various active ingredients that can regulate ferroptosis. As an instance, artesunate, a derivative of artemisinin, can trigger ferroptosis in pancreatic cancer cells by elevating cellular reactive oxygen species and iron accumulation. This, in turn, hinders the growth of cancer cells but does not impact normal cells [24]. Chrysin can up-regulate the expression of Solute Carrier Family 7 Member 11 (*SLC7A11*), GPX4 inhibits the expression of Acyl-CoA Synthetase Long-Chain Family Member 4 (*ACSL4*), Transferrin Receptor 1 (*TFR1*), and Prostaglandin-Endoperoxide Synthase 2 (*PTGS2*), reduce iron overload and oxidative damage, thereby enhancing the damage in a model of transient middle cerebral artery occlusion and inhibiting the ferroptosis of ischemic stroke neurons [25]. Leonurine can inhibit ferroptosis of renal tubular epithelial cells by activating the p62/Nrf2/HO-1 signaling pathway [26]. Baicalein, serving as a specific blocker of arachidonic acid 12/15-lipoxygenase, possesses the capability to shield acute lymphoblastic leukemia cells from ferroptosis instigated by a GPX4 inhibitor [27]. In summary, traditional Chinese medicine and its active ingredients can have a two-way regulatory effect on ferroptosis by targeting different signaling pathways: they can not only positively regulate the occurrence of ferroptosis, but also negatively regulate ferroptosis.

In this paper, high-throughput data were researched by bioinformatics methods. It was found that genes that play a crucial role in IS may include *ALOX5*, *LAMP2*, *MAPK14*, *SLC2A3*, *ABCC1*, *TXN* etc.

Previous studies have found that the activation of *ALOX5*, a vital subtype of *ALOX*, leads to glutamate-induced ferroptosis in immortalized hippocampal neurons HT22. After intervention with *ALOX5* inhibitor Zileuton, neuronal damage is significantly reduced [28], and further research found that Zileuton can reduce intracellular iron content by inhibiting *ALOX5*, averting the ROS and ferroptosis induced by iron clustering [29]. The reduction of *LAMP2* increases the risk of ROS-induced ferroptosis in retinal pigment epithelial cells [30], possibly due to the reduction of cysteine and glutathione. *MAPK14* may induce ferroptosis through the p38/MAPK pathway, and may act as a downstream pathway of lipid peroxide accumulation in ferroptosis [31,32]. *MAPK14* can also affect the level of ROS, which is the direct executor of ferroptosis through *MAPK14/p38 α* [33]. *MAPK14* can affect the level of *SLC2A3*, thereby affecting the glucose level of cells,

which is also closely related to the generation of ROS. MRP1 is a protein transcribed by *ABCC1*, and its high expression level can promote the cell to accelerate the efflux of glutathione, which leads to the occurrence of ferroptosis [34]. Thioredoxin-1, transcribed by the *TXN* gene, also similarly regulates the development of ferroptosis through GPX4 and glutathione [35].

Ferroptosis is also closely related to immunity. Long before ferroptosis was named, it was known that lipid peroxidation was closely related to immune response [36]. Considering T cells as an illustration, being an immune cell originating from the bone marrow and maturing in the thymus, T cells undergo a progression evolving into naive CD4(+) or CD8(+) T cells and migrating to the periphery following a sequence of developmental stages. In the periphery, naive CD4 T cells further undergo distinct differentiations into various T cell subsets. CD8 T cells released interferon to significantly down-regulate *SLC3A2* and *SLC7A11*, the Xc-system during ferroptosis. In the immune process, neutrophils have been shown to have abnormal ferroptosis in colorectal liver metastases. This ferroptosis occurrence in the tumor microenvironment provides the first evidence [37]. Therefore, it is logical to infer that ferroptosis and immune response can interact in specific situations, and explaining the molecular mechanism of immune cell ferroptosis will help to develop new treatment strategies for various diseases [38].

It is also not uncommon to study the regulation of the above genes and proteins by active ingredients of traditional Chinese medicine, single traditional Chinese medicines, or traditional Chinese medicine compounds. Berberine is among the primary active constituents of *Rhizoma Coptidis*, which can promote the expression of *MAPK14* in diabetic model [39]. On the contrary, tripterygium glycosides have the pharmacological effects of immune regulation and anti-inflammation and can express *MAPK14* in animal models of ulcerative colitis [40]. For example, traditional Chinese medicine compounds such as Xinyang Tablets and Chaigui Granules can adjust the expression of *ALOX5* to a certain extent [41,42]. In the animal model of myocardial-ischemia-reperfusion-injury, ginsenoside Rb1 showed the effect of regulating the expression level of *LAMP2* [43].

The screening of related traditional Chinese medicines shows that in the process of ferroptosis of IS, the five flavors of traditional Chinese medicines that play a significant role are primarily bitter, sweet, and pungent. The four Qi are mostly cold and warm, mainly belonging to the liver, lung, stomach, spleen, and kidney, consistent with the clinical commonly used treatment methods for IS. In the early stage of IS development, the main problems were focused on pathological factors such as blood stasis, fire, and phlegm. In contrast, in the later stage of IS development, the contradictions were mainly focused on the deficiency of viscera. For example, academician Wang Yongyan put forward the pathogenesis hypothesis of 'toxin damaging brain collaterals, believing that in the process of IS brain damage, disharmony between Ying and Wei, fire toxin damaging collaterals are the primary pathogenesis of its development [44].

Its treatment should be detoxification and dredging collaterals, combined with bitter and pungent. A study on the distribution of TCM syndromes in IS patients also proved this from the side. In this study, the proportion of patients with fire-heat syndrome was the highest, accounting for 26.6% of all patients [45]. In the later stage of IS development, the problem of deficiency of viscera and vitality energy was gradually revealed. In most IS patients, deficiency is accompanied by pathological factors such as blood stasis. However, at the same time, It is not challenging to observe that visceral insufficiency assumes a

crucial function in the progression of IS. From the data mining results, the components contained in *Zanthoxylum bungeanum*, *Glycyrrhiza uralensis* and *Polygonum cuspidatum* all influence the ferroptosis phenotype [46-49]. *Lygodium japonicum*, *nidus vespa*, ginkgo-nut, Chinese holly leaf, herba geranii, spina gleditsiae, euphorbia lunulata, curcumae radix, semen armeniacae amarum, and their active ingredients have antioxidant and anti-inflammatory effects [50-58]. These drugs may regulate ferroptosis by inhibiting lipid peroxidation or inflammation-related ferroptosis, and their specific effects remain to be explored.

The outcomes of molecular docking indicated that the primary Chinese herbal remedies and their active small molecules for treating IS primarily restrained lipid peroxidation or ferroptosis linked to inflammation through targets such as *ECH1*, *ALOX5*, and *SLC2A3*. In particular, for *ECH1* targets, molecular dynamics results showed that *ECH1*-Kaempferol-3,7-O-bis- α -L-rhamnoside, *ECH1*-118705169, and other receptor-ligand complex systems have the characteristics of high binding affinity, stable binding process, and similar drug onset sites, which have the value of further studying the molecular mechanism.

In summary, based on modern methods, traditional Chinese medicine is systematically summarized, analyzed, and combined with pharmacological experiments. Then the effective drugs that can act on the ferroptosis process in the development of IS disease are screened from the traditional Chinese medicine components, which will offer novel insights and a theoretical foundation for the advancement and utilization of traditional Chinese medicine and the exploration of new drugs associated with IS based on the ferroptosis mechanism, subsequently presenting an innovative approach for the challenging treatment of IS in clinical practice.

Conclusion

In this investigation, bioinformatics techniques were employed to scrutinize the association of ferroptosis in the IS data from the GEO database, and it was concluded that there was a significant correlation between ferroptosis and IS. The drugs that play a significant role in this process are mainly bitter and cold, followed by sweet and warm products, which mainly regulate the liver, lung, stomach, spleen, and other viscera, play the role of clearing heat and detoxifying, sweet and warm tonic, and interfere with ferroptosis by inhibiting lipid peroxidation or inflammation. The outcomes of molecular docking, along with molecular dynamics, indicated that the receptor-ligand complex systems such as *ECH1*-Kaempferol-3,7-O-bis- α -L-rhamnoside and *ECH1*-118705169 were more stable, which had the value of further studying the molecular mechanism. This study can offer reference and guidance for the practical implementation and further exploration of traditional Chinese medicine.

Declarations

This study did not involve clinical patients or their biological samples, therefore there is no need for an Ethical statement/Clinical trial registration number/Informed consent.

Funding

This work was supported by Tianjin Municipal Science and Technology Committee (2018KJ033).

Author Contribution

Changzhong WANG and Zijin SUN wrote the main manuscript

text and prepared figures and tables. Wei ZHOU Provided fund support. All authors reviewed the manuscript.

Availability of Data and Materials

All data can be retrieved and obtained from the database mentioned in the article by using the dataset number in the article index.

References

- Dixon SJ, Lemberg KM, Lamprecht MR, Skouta R, Zaitsev EM, et al. (2012) Ferroptosis: an iron-dependent form of nonapoptotic cell death. *Cell* 149:1060-1072.
- Yang WS, Stockwell BR (2008) Synthetic lethal screening identifies compounds activating iron-dependent, nonapoptotic cell death in oncogenic-ras-harboring cancer cells. *Chemistry & Biology* 15:234-245.
- Doll S, Conrad M (2017) Iron and ferroptosis: a still ill-defined liaison. *IUBMB Life* 69:423-434.
- Kagan VE, Mao G, Qu F, Angeli JP, Doll S, et al. (2017) Oxidized arachidonic and adrenic peptides navigate cells to ferroptosis. *Nature Chemical Biology* 13:81-90.
- Yagoda N, von Rechenberg M, Zaganjor E, Bauer AJ, Yang WS, et al. (2007) RAS-raf-mek-dependent oxidative cell death involving voltage-dependent anion channels. *Nature* 447: 864-868.
- Tang D, Chen X, Kang R, Kroemer G (2021) Ferroptosis: molecular mechanisms and health implications. *Cell Res* 31:107-125.
- Wu J-R, Tuo Q-Z, Lei P (2018) Ferroptosis, a recently defined form of critical cell death in neurological disorders. *Journal of molecular neuroscience* 66:197-206.
- Li X, Zeng J, Liu Y, Liang M, Liu Q, et al. (2020) Inhibitory effect and mechanism of action of quercetin and quercetin diols-alder anti-dimer on erastin-induced ferroptosis in bone marrow-derived mesenchymal stem cells. *Antioxidants* 9:205.
- Liu B, Zhao C, Li H, Chen X, Ding Y, et al. (2018) Puerarin protects against heart failure induced by pressure overload through mitigation of ferroptosis. *Biochemical and Biophysical Research Communications* 497: 233-240.
- Jiang T, Cheng H, Su J, Wang X, Wang Q, et al. (2020) Gastrodin protects against glutamate-induced ferroptosis in ht-22 cells through nrf2/ho-1 signaling pathway. *Toxicology in vitro* 62:104715.
- Randolph S A (2016) Ischemic stroke. *Workplace Health & Safety* 64: 444
- Hay SI, Abajobir AA, Abate KH, Abbafati C, Abbas KM, et al. (2017) Global, regional, and national disability-adjusted life-years (DALYs) for 333 diseases and injuries and healthy life expectancy (HALE) for 195 countries and territories, 1990-2016: a systematic analysis for the Global Burden of Disease Study 2016. *Lancet* 390:1260-344.
- Wan J, Ren H, Wang J (2019) Iron toxicity, lipid peroxidation and ferroptosis after intracerebral haemorrhage. *Stroke and Vascular Neurology* 4:93-95.
- Lipscomb DC, Gorman LG, Traystman RJ, Hum PD (1998) Low molecular weight iron in cerebral ischemic acidosis *in vivo*. *Stroke* 29:487-492.
- Almutairi M M A, Xu G, Shi H (2019) Iron pathophysiology in stroke. *Advances in Experimental Medicine and Biology* 1173: 105-123.

16. Hanafy K A, Gomes J A, Selim M (2019) Rationale and current evidence for testing iron chelators for treating stroke. *Current Cardiology Reports* 21:20.
17. Zhao Y, Xin Z, Li N, Chang S, Chen Y, et al. (2018) Nano-liposomes of lycopene reduces ischemic brain damage in rodents by regulating iron metabolism. *Free Radical Biology & Medicine* 124: 1–11.
18. DeGregorio-Rocasolano N, Martí-Sistac O, Gasull T (2019) Deciphering the iron side of stroke: neurodegeneration at the crossroads between iron dyshomeostasis, excitotoxicity, and ferroptosis. *Frontiers in Neuroscience* 13:85.
19. Tuo QZ, Lei P, Jackman KA, Li XL, Xiong H, et al. (2017) Tau-mediated iron export prevents ferroptotic damage after ischemic stroke. *Molecular Psychiatry* 22:1520–1530.
20. van Etten ES, van der Grond J, Dumas EM, van den Bogaard SJ, van Buchem MA, et al. (2015) MRI susceptibility changes suggestive of iron deposition in the thalamus after ischemic stroke. *Cerebrovascular Diseases* 40:67-72.
21. García-Yébenes I, Sobrado M, Moraga A, Zaruk JG, Romera VG, et al. (2012) Iron overload, measured as serum ferritin, increases brain damage induced by focal ischemia and early reperfusion. *Neurochemistry International* 61:1364–1369.
22. Li L, Li YW, Zhao JY, Liu YZ, Holscher C (2009) Quantitative analysis of iron concentration and expression of ferroportin 1 in the cortex and hippocampus of rats induced by cerebral ischemia. *Journal of Clinical Neuroscience* 16:1466–1472.
23. Petrova J, Manolov V, Vasilev V, Tzatchev K, Marinov B (2016) Ischemic stroke, inflammation, iron overload - connection to a hepcidin. *International Journal of Stroke* 11:NP16-17.
24. Yu Y, Xie Y, Cao L, Yang L, Yang M, et al. (2015) The ferroptosis inducer erastin enhances sensitivity of acute myeloid leukemia cells to chemotherapeutic agents. *Molecular & Cellular Oncology* 2:e1054549.
25. Shang JF, Jiao JK, Li QN, Lu YH, Wang JY, et al. (2023) Chrysin alleviates cerebral ischemia-reperfusion injury by inhibiting ferroptosis in rats. *China Journal of Chinese Materia Medica* 48:1597-605.
26. Wu AJ, Chen NQ, Huang LH, Cheng R, Wang XW, et al. (2023) Leonurine inhibits ferroptosis in renal tubular epithelial cells by activating p62/Nrf2/HO-1 signaling pathway. *China Journal of Chinese Materia Medica* 48:2176-83.
27. Probst L, Dächert J, Schenk B, Fulda S (2017) Lipoxygenase inhibitors protect acute lymphoblastic leukemia cells from ferroptotic cell death. *Biochemical Pharmacology* 140:41-52.
28. Liu Y, Wang W, Li Y, Xiao Y, Cheng J, et al. (2015) The 5-lipoxygenase inhibitor zileuton confers neuroprotection against glutamate oxidative damage by inhibiting ferroptosis. *Biological & Pharmaceutical Bulletin* 38:1234-1239.
29. Xie Y, Hou W, Song X, Yu Y, Huang J, et al. (2016) Ferroptosis: process and function. *Cell Death & Differentiation* 23:369-79.
30. Lee JJ, Ishihara K, Notomi S, Efstathiou NE, Ueta T, et al. (2020) Lysosome-associated membrane protein-2 deficiency increases the risk of reactive oxygen species-induced ferroptosis in retinal pigment epithelial cells. *Biochemical and Biophysical Research Communications* 521:414-419.
31. Li L, Hao Y, Zhao Y, Wang H, Zhao X, et al. (2018) Ferroptosis is associated with oxygen-glucose deprivation/reoxygenation-induced sertoli cell death. *International Journal of Molecular Medicine* 41:3051-3062.
32. Hattori K, Ishikawa H, Sakauchi C (2017) Cold stress-induced ferroptosis involves the ask1-p38 pathway. *EMBO Reports* 18:2067-2078.
33. Desideri E, Vegliante R, Cardaci S, Nepravishta R, Paci M, et al. (2014) MAPK14/p38 α -dependent modulation of glucose metabolism affects ros levels and autophagy during starvation. *Autophagy* 10:1652–1665.
34. Cao JY, Poddar A, Magtanong L, Lumb JH, Mileur TR, et al. (2019) A genome-wide haploid genetic screen identifies regulators of glutathione abundance and ferroptosis sensitivity. *Cell Reports* 26:1544-1556.e8.
35. Bai L, Yan F, Deng R, Gu R, Zhang X, et al. (2021) Thioredoxin-1 rescues mpp+/mptp-induced ferroptosis by increasing glutathione peroxidase. *Molecular Neurobiology* 58:3187–3197.
36. Weismann D, Binder CJ (2012) The innate immune response to products of phospholipid peroxidation. *Biochim Biophys Acta* 1818:2465-75.
37. Zhang Y, Song J, Zhao Z, Yang M, Chen M, et al. (2020) Single-cell transcriptome analysis reveals tumor immune microenvironment heterogeneity and granulocytes enrichment in colorectal cancer liver metastases. *Cancer letters* 470:84-94.
38. Xu S, Min J, Wang F (2021) Ferroptosis: an emerging player in immune cells. *Sci Bull* 66:2257-60.
39. Pirillo A, Catapano AL (2015) Berberine, a plant alkaloid with lipid- and glucose-lowering properties: from *in vitro* evidence to clinical studies. *Atherosclerosis* 243:449-61.
40. Zhao L, Lan Z, Peng L, Wan L, Liu D, et al. (2022) Triptolide promotes autophagy to inhibit mesangial cell proliferation in IgA nephropathy via the CARD9/p38 MAPK pathway. *Cell Proliferation* 55:e13278.
41. Tian JS, Wu ZN, Wu D, Yang C, Gao Y, et al. (2023) Combining network pharmacology and experimental verification to reveal the mechanism of Chaigui granules in the treatment of depression through PI3K/Akt/mTOR signaling pathways. *Metabolic Brain Disease* 38:2849-64.5
42. Gao AR, Li S, Tan XC, Huang T, Dong HJ, et al. (2022) Xinyang Tablet attenuates chronic hypoxia-induced right ventricular remodeling via inhibiting cardiomyocytes apoptosis. *Chinese Medicine* 17:134.
43. Zheng Q, Bao XY, Zhu PC, Tong Q, Zheng GQ, et al. (2017) Ginsenoside Rb1 for myocardial ischemia/reperfusion injury: Preclinical evidence and possible mechanisms. *Oxid Med Cell Longev* 2017:6313625.
44. Zhou L, Zhang YL, Hou XB, Hu H (2012) Senile dementia: differentiation of syndromes according to meridians based on the theory of "cerebral collaterals injury by toxin. *Chinese Acupuncture & Moxibustion* 32:1031-4.
45. You JS, Huang Y, Cai YF, Guo JW, Liang WX, et al. (2008) Characteristics of traditional Chinese medicine syndromes in patients with acute ischemic stroke of yin or yang syndrome: a multicenter trial. *Journal of Chinese Integrative Medicine* 6:346-51.
46. Zhu T, Wang L, Wang LP, Wan Q (2022) Therapeutic targets of neuroprotection and neurorestoration in ischemic stroke: Applications for natural compounds from medicinal herbs. *Biomed Pharmacother* 148:112719.
47. Tang Y, Luo H, Xiao Q, Li L, Zhong X, et al. (2021) Isoliquiritigenin attenuates septic acute kidney injury by regulating ferritinophagy-mediated ferroptosis. *Renal failure* 43:1551-60.
48. Chen ZQ, Sun XH, Li XJ, Xu ZC, Yang Y, et al. (2020) Polydatin attenuates renal fibrosis in diabetic mice through regulating the Cx32-Nox4 signaling pathway. *Acta Pharmacologica Sinica* 41:1587-96.

-
49. Zhang KF, He PY, He DH (2020) Study on isobutyl amide compounds from *Zanthoxylum bungeanum* and their activities against ferroptosis in HT22 hippocampal cells. *Natural Product Research and Development* 32:18-22.
50. Li Y, Sheng Y, Liu J, Xu G, Yu W, et al. (2022) Hair-growth promoting effect and anti-inflammatory mechanism of Ginkgo biloba polysaccharides. *Carbohydrate Polymers* 278:118811.
51. Li XL, Zhou AG, Han Y (2006) Anti-oxidation and anti-microorganism activities of purification polysaccharide from *Lygodium japonicum* *in vitro*. *Carbohydrate Polymers* 66:34-42.
52. Zhu M, Han W, Ling Y, Qi Q, Zhang Y, et al. (2021) Preliminary study on the *in vitro* antitumor effects of nidus vespae on gastric cancer. *Evidence-Based Complementary and Alternative Medicine* 2021:1-9.
53. Wang B, Wei PW, Wan S, Yao Y, Song CR, et al. (2021) Ginkgo biloba exocarp extracts inhibit *S. aureus* and *MRSA* by disrupting biofilms and affecting gene expression. *Journal of Ethnopharmacology* 271:113895.
54. Wang Y, Yu X, Wang L, Zhang F, Zhang Y (2020) Research progress on chemical constituents and Anticancer pharmacological activities of *Euphorbia lunulata* Bunge. *Biomed Res Int* 2020:3618941.
55. Gao J, Yang X, Yin W (2016) From traditional usage to pharmacological evidence: A systematic mini-review of spina gleditsiae. *Evid Based Complement Alternat Med* 2016:3898957.
56. Kong C, Pang X, Su Z, Liu Y (2023) Botany, ethnopharmacology, phytochemistry and pharmacology of Erodii Herba Geranii Herba-An review. *J Ethnopharmacol* 302:115858.
57. Ao M, Li X, Liao Y, Zhang C, Fan S, et al. (2022) Curcumae Radix: a review of its botany, traditional uses, phytochemistry, pharmacology and toxicology. *Journal of Pharmacy and Pharmacology* 74:779-92.
58. Do JS, Hwang JK, Seo HJ, Woo WH, Nam SY (2006) Antiasthmatic activity and selective inhibition of type 2 helper T cell response by aqueous extract of semen armeniacae amarum. *Immunopharmacol Immunotoxicol* 28:213-225.